Supplementary information

Finely tuning the phosphorus active site on g-C$_3$N$_4$ nanosheets for enhanced photocatalytic decontamination

Lian-Lian Liu[a],*, Fei Chen[a,b,c],*, Jing-Hang Wu[a], Wen-Wei Li[a], Jie-Jie Chen[a],**, Han-Qing Yu [a],**

[a]CAS Key Laboratory of Urban Pollutant Conversion, Department of Environmental Science and Engineering, University of Science & Technology of China, Hefei, China

[b]Key Laboratory of the Three Gorges Reservoir Region's Eco-Environment, Ministry of Education, Chongqing University, Chongqing, 400045, China

[c]College of Environment and Ecology, Chongqing University, Chongqing, 400045, China

* These authors contributed equally to this work.

**Corresponding authors:

Prof. Jie-Jie Chen, Fax: 86-551-63601592, E-mail: chenjiej@ustc.edu.cn

Prof. Han-Qing Yu, Fax: 86-551-63607592, E-mail: hqyu@ustc.edu.cn

Experimental method section

Photoelectrochemical characterizations

The CHI660E electrochemical workstation equipped with a standard three-electrode system was used to characterize the photoelectrochemical characteristics of the prepared photocatalysts. The reference electrode is a saturated Ag/AgCl electrode, the counter electrode is a platinum wire, and the working electrode is an F-doped SnO_2 (FTO) conductive glass covered with the photocatalyst. The working electrode was prepared as follows: first, 5 mg sample was dispersed into a mixed solution containing ethanol (0.3 mL) and isopropanol (0.1 mL) under the ultrasonication treatment for 30 min. Then the stored Nafion solution (20 μL) was added into the suspension and sonicated for another 30 min. Finally, the formed ink (0.2 mL) was coated onto a 1 cm×4 cm FTO with an effective working area of 2 cm^2 and dried at 200 ℃ for 2 h. A 300 W Xe lamp (PLS/SXE 300D/300DUV, Beijing Perfectlight Technology Co., Ltd.) with a 400 nm cutoff filter was used as the light source. The transient photocurrent response curve was measured under a bias voltage of 0 V and 0.25 M Na_2SO_4 aqueous solution was used as the electrolyte. Electrochemical impedance spectroscopy (EIS) was obtained by applying an AC voltage of 5 mV amplitude in the frequency range from 10^5 to 1 Hz and the aqueous solution (containing 5 mM $[Fe(CN)_6]^{3-/4-}$ and 0.1 M KCl) served as the electrolyte. Mott-Schottky plots were carried out at a frequency of 1 kHz and the applied voltage range of -1.5-0 V.
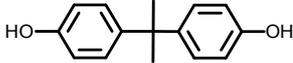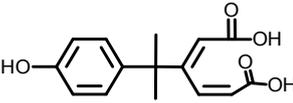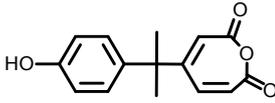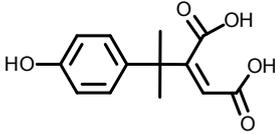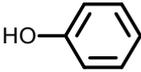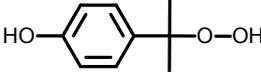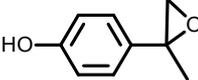
Active species trapping and ESR measurements

Before light reaction, various scavengers were dosed into BPA solution to investigate the reactive

species involved in the photocatalytic reaction. Benzoquinone (BQ), sodium thiosulfate ($Na_2S_2O_3$), isopropanol (IPA), and sodium oxalate ($Na_2C_2O_4$) were respectively selected as the scavengers of superoxide radical ($\cdot O_2^-$), electron (e^-), hydroxyl radical ($\cdot OH$) and holes (h^+). To investigate the source of O_2, the catalytic reaction under N_2 saturated conditions were conducted. Additionally, the formation of $\cdot O_2^-$ and $\cdot OH$ radicals was further validated by electron spin resonance (ESR) spin-trapping spectra with reagent 5, 5-dimethyl-l-pyrroline N-oxide (DMPO) as the trapping agent (ER200-SRC, Bruker Co., USA). The as-prepared photocatalyst of 5 mg was first dissolved into 0.5 mL of methanol for the DMPO-$\cdot O_2^-$ or 0.5 mL of deionized water for the DMPO-$\cdot OH$, then 10 µL DMPO was dosed and the ESR signals were obtained under the conditions of both dark and visible light irradiation.

Table S1. BET surface area of the prepared photocatalysts.

Photocatalyst	BET Surface Area (m^2/g)	Pore Volume (cm^3/g)	Pore Size (nm)
bulk gCN	9.956	0.0798	32.1
P-gCN	5.596	0.0521	57.2
gCN nanosheets	135.1	0.6273	18.6
gCN-P (post)	92.68	0.5106	22.0

Table S2. Intermediates for the photocatalytic degradation of BPA by gCN-P (post).

Product	m/z	Structural formula
BPA	227	
Item A	275	
Item B	257	
Item C	261	
Item D	93	
Item E	167	
Item F	149	
Item G	135	
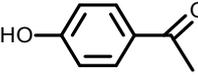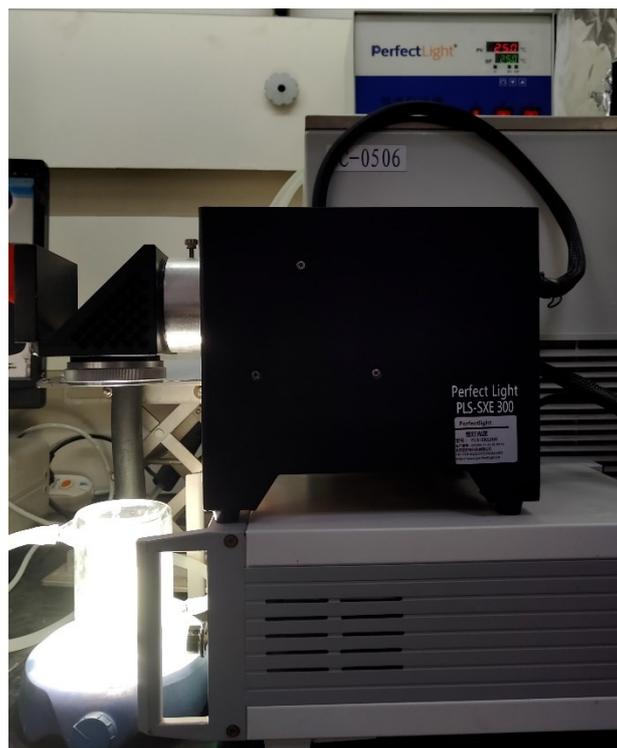
Fig. S1. Schematic diagram of the photocatalytic degradation reaction.
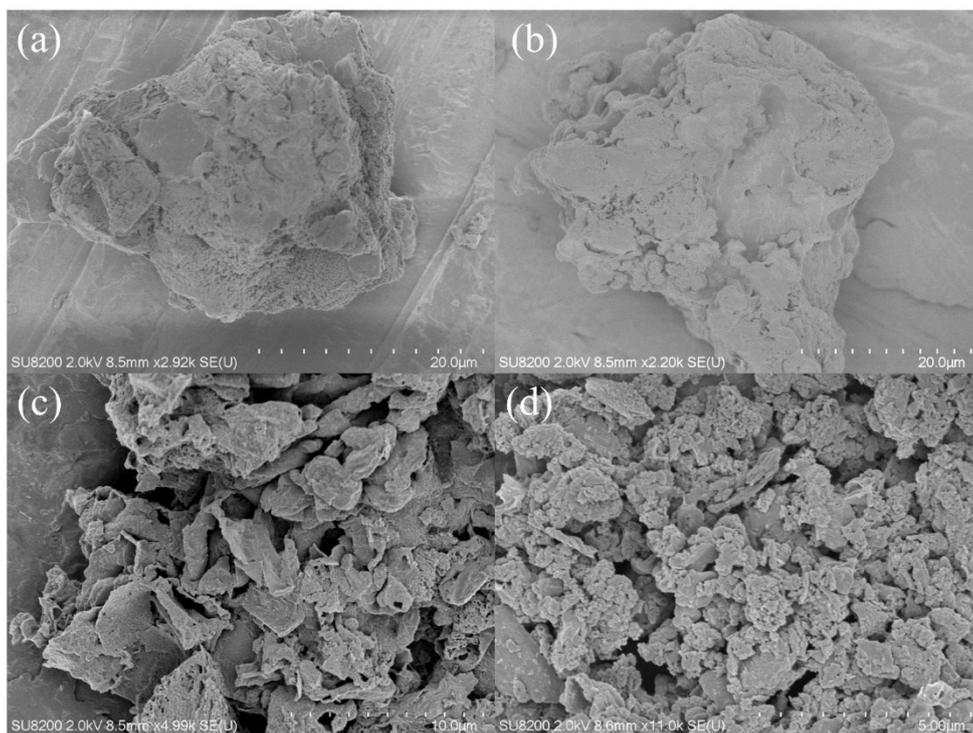
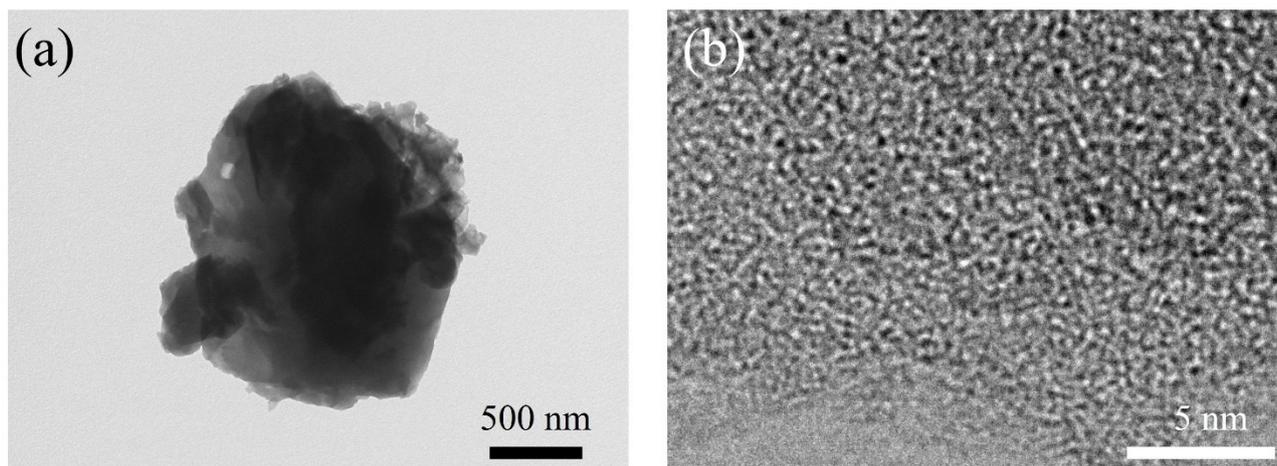**Fig. S2** SEM images of (a) gCN bulk, (b) P-gCN, (c) gCN sheet, and (d) gCN-P (post)

Fig. S3 (a) TEM and (b) HRTEM images of P-gCN.
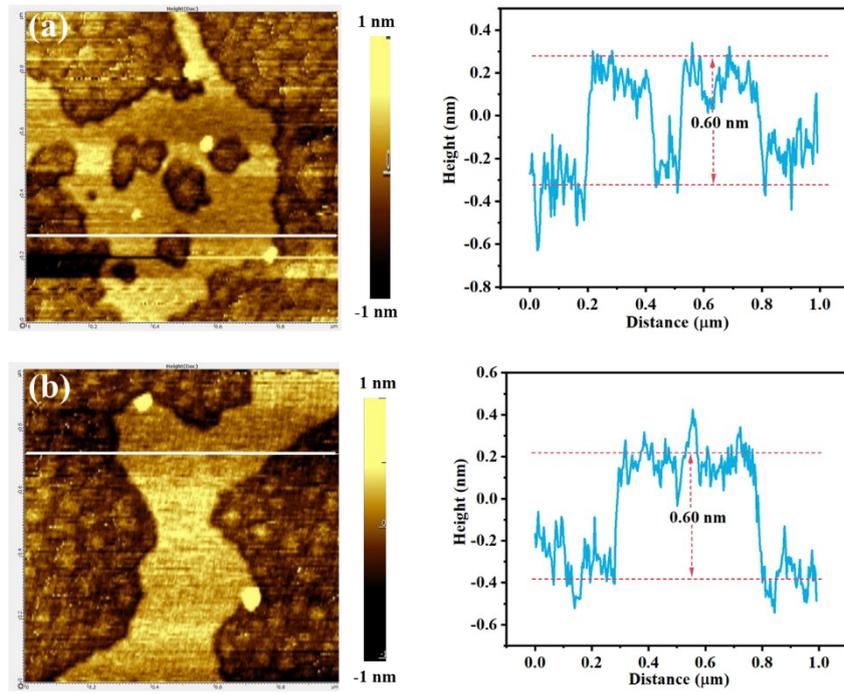
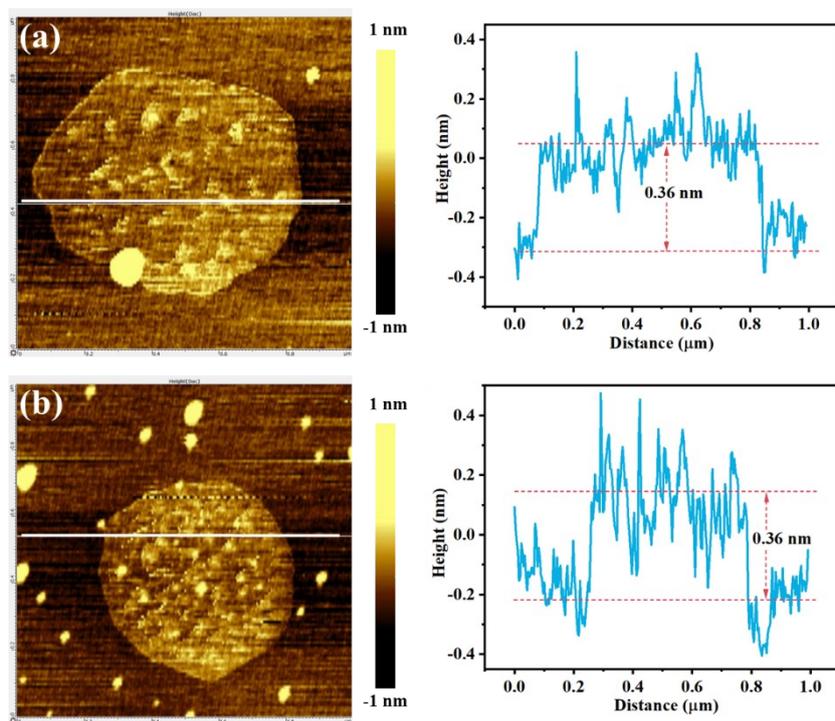Fig. S4. AFM images and the height distribution profiles of gCN sheet (a-b).

Fig. S5. AFM images and the height distribution profiles of gCN-P (a-b).
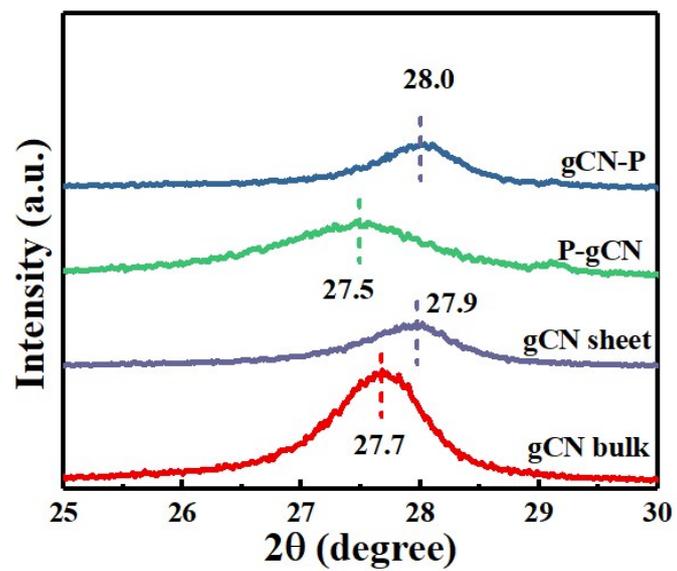
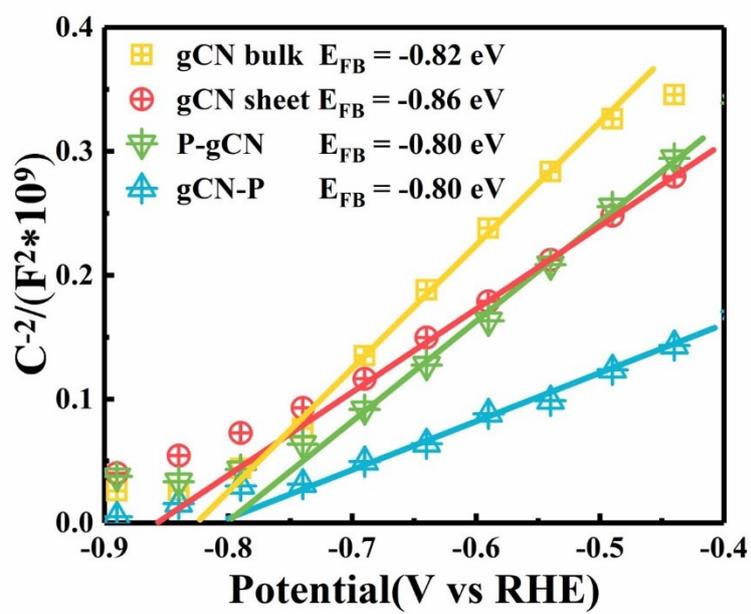**Fig. S6.** The enlarged view of the (002) peak in the XRD patterns of the prepared samples.

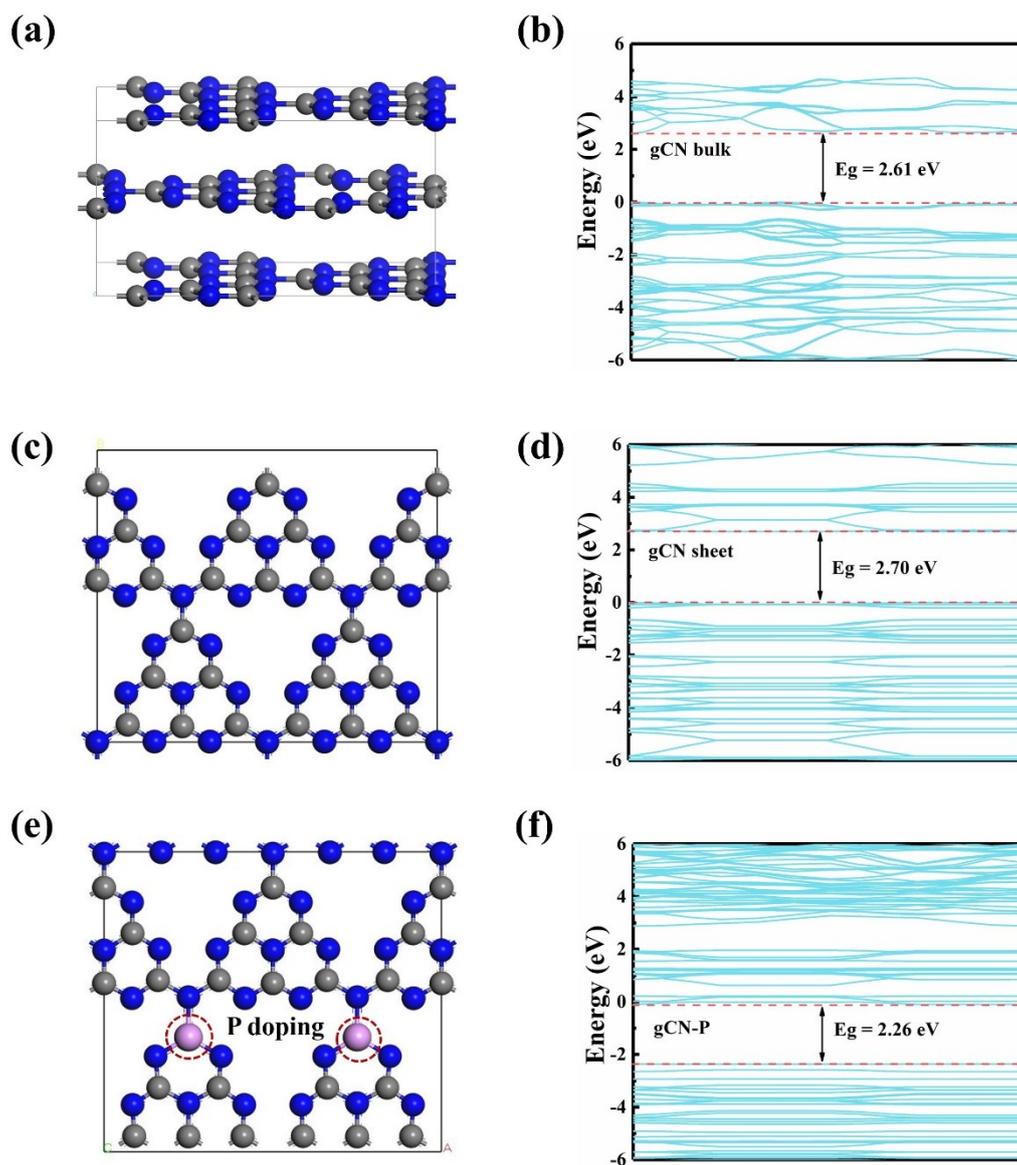**Fig. S7.** Mott−Schottky plots of gCN bulk, gCN sheet, P-gCN, and gCN-P (post).

Fig. S8. Optimized geometric structure of (a) gCN bulk, (c) gCN sheet and (e) gCN-P (post). Band structure of (b) gCN bulk, (d) gCN sheet and (f) gCN-P (post).
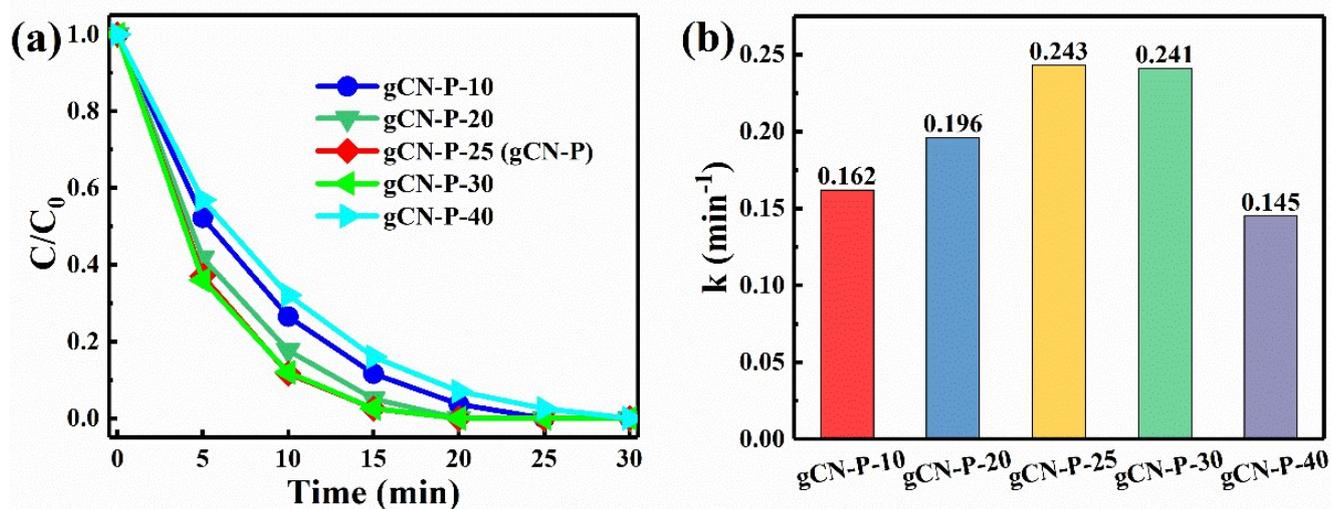
Fig. S9. (a) Photocatalytic degradation of BPA by the photocatalysts with different P loadings under visible light irradiation and (b) the relative reaction kinetic data.
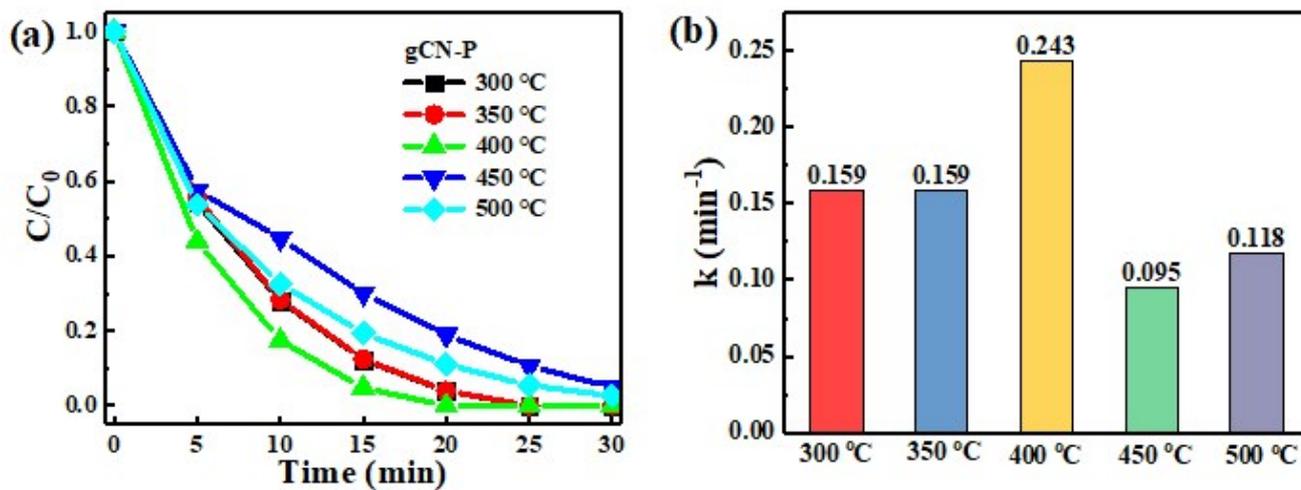
Fig. S10. (a) Photocatalytic degradation of BPA by the photocatalysts obtaining from different calcination temperatures under visible light irradiation and (b) the relative reaction kinetic data.
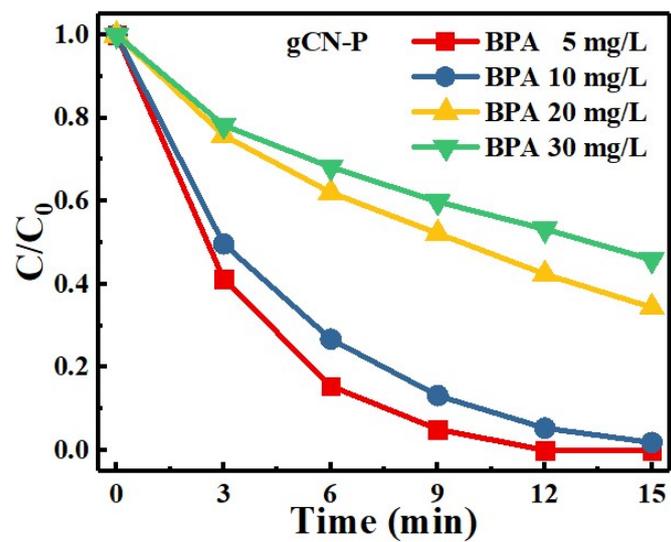
Fig. S11. Photocatalytic degradation of BPA with different initial concentrations over the gCN-P (post) under visible light irradiation.
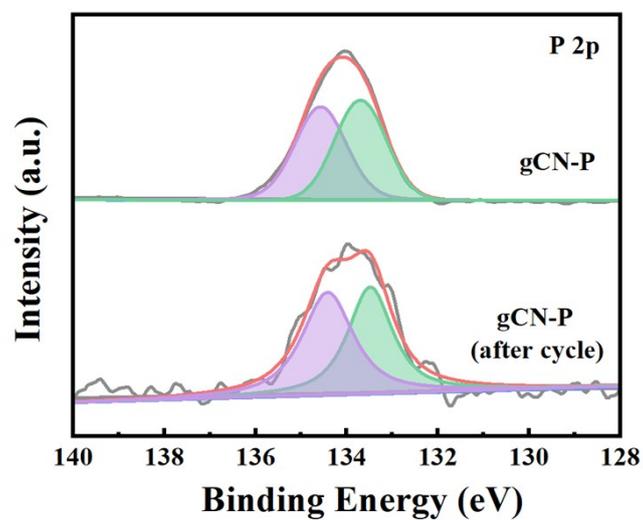
Fig. S12. Comparison of P 2p high-resolution XPS spectra of the gCN-P (post) before and after cycling experiments.
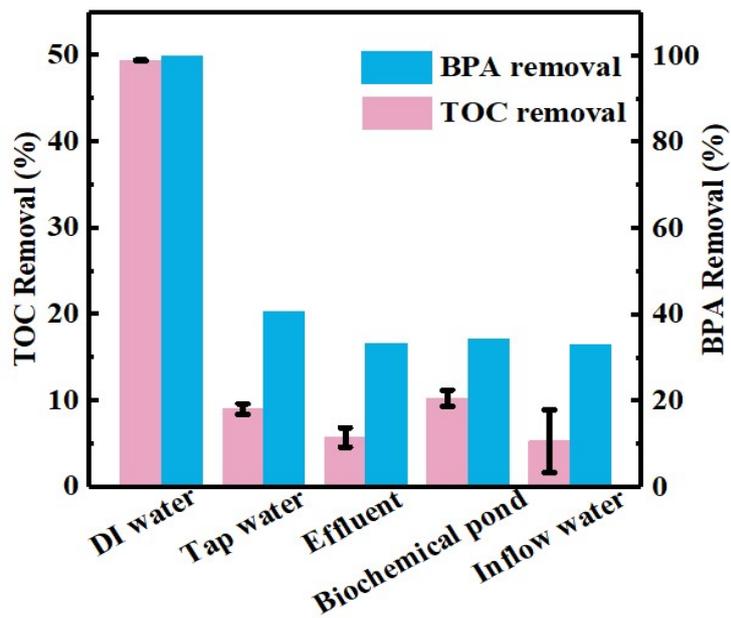
Fig. S13. TOC and BPA removals using different water sources by the gCN-P (post) photocatalyst under visible light irradiation with the reaction time of 15 min.
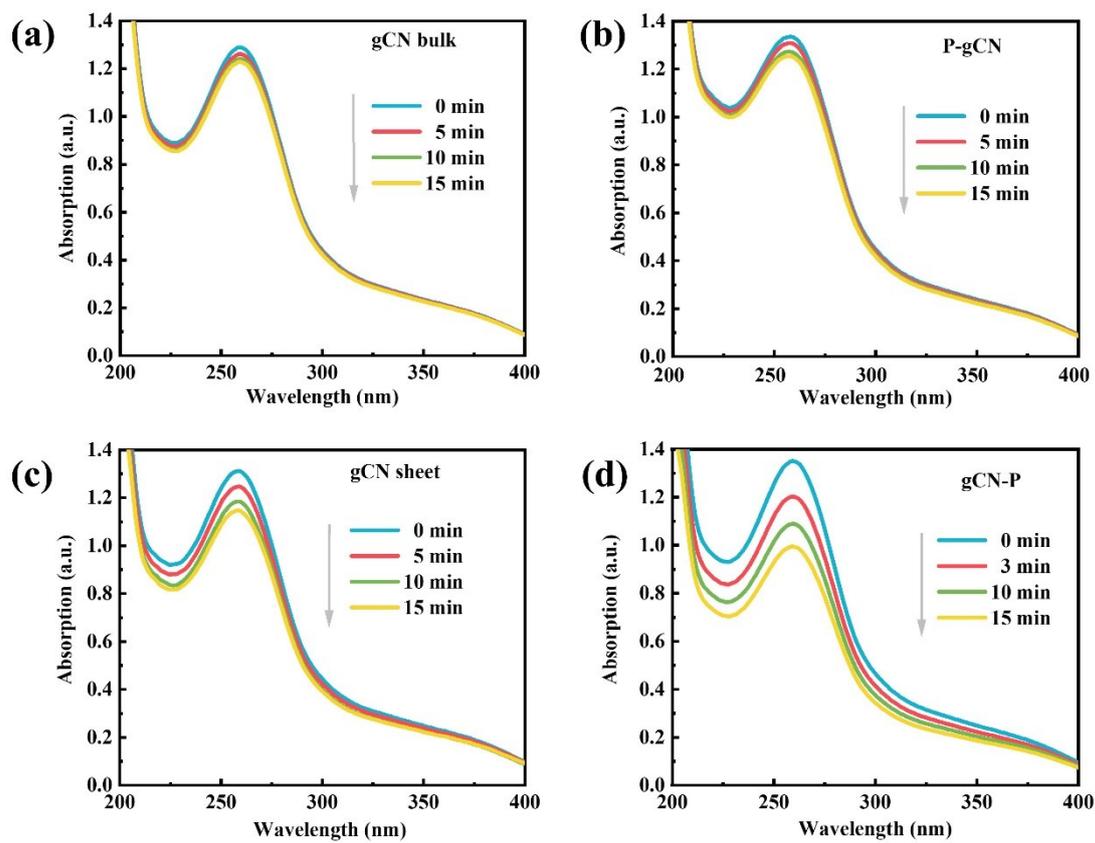
Fig. S14. UV absorption variations of NBT at 259 nm in the presence of (a) gCN bulk, (b) P-gCN, (c) gCN sheet and (d) gCN-P.
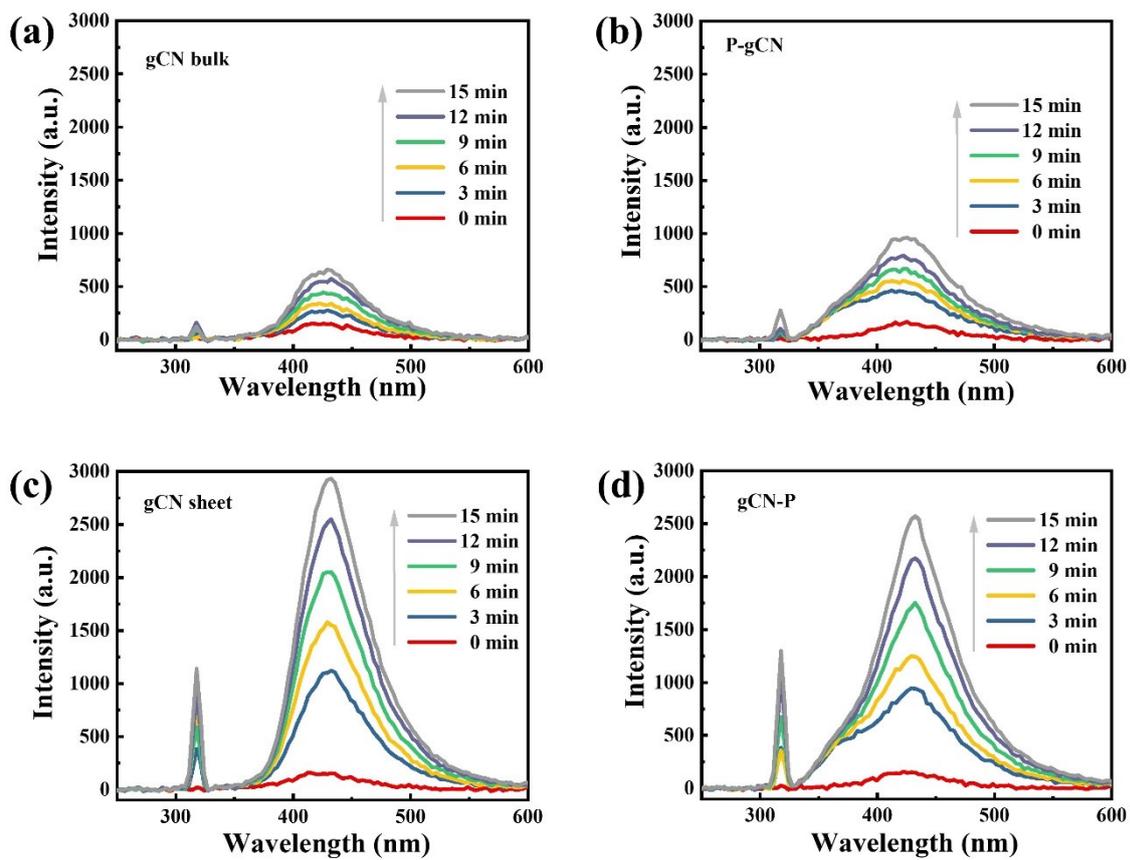
Fig. S15. Fluorescent response variations of TAOH in the presence of (a) gCN bulk, (b) P-gCN, (c) gCN sheet and (d) gCN-P.